Ni Yao[1], Yanhui Tian[1], Daniel Gama das Neves[2, 3], Chen Zhao[4], Claudio Tinoco Mesquita[2], Wolney de Andrade Martins[3, 5], Alair Augusto Sarmet Moreira Damas dos Santos[2, 3], Yanting Li[1], Chuang Han[1], Fubao Zhu[1], Neng Dai[6, 7], Weihua Zhou[4, 8]

[1] Zhengzhou University of Light Industry, School of Computer Science and Technology, Zhengzhou, Henan, China
[2] Universidade Federal Fluminense, Department of Radiology, Rio de Janeiro State, Brazil
[3] DASA Complexo Hospitalar de Niterói, Rio de Janeiro State, Brazil
[4] Michigan Technological University, Department of Applied Computing, Houghton, MI, USA
[5] Universidade Federal Fluminense, Department of Cardiology, Rio de Janeiro State, Brazil
[6] Zhongshan Hospital, Fudan University, Shanghai Institute of Cardiovascular Diseases, Department of Cardiology, Shanghai, China
[7] National Clinical Research Center for Interventional Medicine, Shanghai, China
[8] Center for Biocomputing and Digital Health, Institute of Computing and Cybersystems, and Health Research Institute, Michigan Technological University, Houghton, MI, USA

# Incremental Value of Radiomics Features of Epicardial Adipose Tissue for Detecting the Severity of COVID-19 Infection

## Additional materials

### Supplementary Methods

#### *Study Population*

For the EAT extraction study, the heart contour of 47 subjects in Cohort 1 (27 mild and 20 severe COVID-19 cases) and 15 subjects in Cohort 2 (8 mild and 7 severe COVID-19 cases) was manually drawn by experienced operators on LabelMe (Version 4.5.9) and used to train the segmentation model. For the classification modeling phase of mild and severe cases, the EAT of the remaining 368 subjects from Cohort 1 and 85 subjects from Cohort 2 was extracted automatically using a trained deep learning model. 415 patients (371 mild cases and 44 severe cases) with confirmed COVID-19 from Cohort 1 were randomly divided into a derivation Cohort (n=290, 260 mild cases, 30 severe cases) and an internal validation cohort (n=125, 111 mild cases, 14 cases) (Figure 1). Each case contained its clinical information and a set of chest computed tomography (CT) images in Cohort 1. 100 patients (50 mild and 50 severe) from Cohort 2 were deemed as an external validation cohort (Figure 1). Each case contains a set of chest CT images in Cohort 2.

### Supplementary Results

#### *Patient characteristics*

In the internal validation cohort, 14 (11.2%) patients were diagnosed with severe COVID-19. The mean age of mild and severe cases was 40.46±15.23 yrs and 59.71±14.46 yrs, respectively, and 59% (n=111) and 79% (n=14) were male, respectively (Table 1). There were no significant differences (p>0.05) in gender, white blood cell count, lactic acid, and creatinine.

Fifty patients (50%) were diagnosed with severe COVID-19 in the external validation cohort. The mean age of mild and severe cases was 46.22±7.38 and 62.38±16.14 yrs, respectively, and 56% (n=28) and 60% (n=30) were male, respectively. There were no significant differences (p>0.05) in gender.

#### *Chest CT procedures*

CT scans were performed using Toshiba Aquilion 64 CT scanner in Cohort 1. Image acquisition parameters consisted of 120 kV and 114.1 mAs. The thickness of the CT scanned slices was 5 mm, and the in-plane pixel size ranged from 0.579 mm to 0.935 mm. The number of chest CT slices for each patient ranged from 52 to 70. CT scans were performed using a Siemens Somatom Sensation 64 CT scanner in Cohort 2. Image acquisition parameters consisted of 120 kV and 94 mAs. The thickness of the CT scanned slices was 1 mm, and the in-plane pixel size ranged from 0.669 mm to 0.815 mm. The number of chest CT slices for each patient ranged from 300 to 370.

Due to the difference in CT data acquisition imaging between the two cohorts, the segmentation method was used to train the model in the two cohorts.

### Supplementary Discussion

#### *EAT segmentation*

A comparative test was conducted with a three-dimensional V-Net [27] network to explore whether object detection combined with a two-dimensional network would enhance segmentation (Figure 3). The experimental results revealed that while the 3D network can avoid the need to select CT images by object detection, its accuracy in

**Supplementary Table 1.** Baseline characteristics of patients in the derivation and internal validation cohort with mild and severe COVID-19

| Characteristics | Derivation Cohort | | p | Internal Validation Cohort | | p |
|---|---|---|---|---|---|---|
| | Mild | Severe | | Mild | Severe | |
| Age, yrs | 39.98±15.39 | 59.23±14.86 | <.001 | 40.46±15.23 | 59.71±14.46 | <.001 |
| Gender | | | 59 | | | 15 |
| Male | 125 (48) | 16 (53) | | 65 (59) | 11 (79) | |
| Female | 135 (52) | 14 ( 47) | | 46 (41) | 3 (21) | |
| Past cardiovascular disease | 35 (13) | 13 ( 43) | <.001 | 16 (14) | 5 (36) | .045 |
| Lactate dehydrogenase, (U/l) | 219.37±61.10 | 346.47±142.47 | <.001 | 220.29±83.26 | 326.29±102.63 | <.001 |
| NTPro-BNP, (pg/ml) | 4.22±0.94 | 4.19±1.01 | .84 | 4.26±0.83 | 3.71±0.62 | .02 |
| Creatine kinase isoenzymes, (ng/ml) | 13.19±12.07 | 16.43±10.69 | .16 | 12.61±4.66 | 12.91±2.37 | .82 |
| Hypertension, | 31 (12) | 9 (30) | .01 | 16(14) | 5 (36) | .045 |
| D-dimer, (ug/ml) | 0.55±1.34 | 1.72±3.70 | <.001 | 0.57±1.64 | 2.23±4.96 | .01 |
| White blood cell, ($10^9$/l) | 5.55±1.90 | 5.37±1.94 | .61 | 5.38±2.39 | 6.22±4.61 | .29 |
| Lymphocyte, ($10^9$/l) | 1.44±0.60 | 1.02±0.41 | <.001 | 1.45±0.49 | 0.93±0.61 | <.001 |
| Serum sodium, (mmol/l) | 139.90±2.70 | 137.70±3.77 | <.001 | 139.98±2.04 | 134.29±5.20 | <.001 |
| Urea, (mmol/l) | 4.43±1.50 | 5.56±3.46 | <.001 | 4.43±1.13 | 5.04±2.09 | .09 |
| PO2, (KPa) | 14.34±4.34 | 9.94±4.94 | <.001 | 14.68±4.75 | 13.45±5.51 | .38 |
| PCO2, (KPa) | 5.43±0.45 | 5.49±0.89 | .66 | 5.39±0.59 | 4.94±0.72 | .01 |
| PCT, (ng/ml) | 0.04±0.03 | 0.18±0.39 | <.001 | 0.04±0.04 | 0.16±0.18 | <.001 |
| APTT, (s) | 38.57±6.35 | 42.06±6.57 | .01 | 38.02±4.10 | 43.10±5.69 | <.001 |
| PT, (s) | 13.38±1.10 | 13.62±0.83 | .26 | 13.29±0.60 | 13.73±1.46 | .04 |
| Potassium, (mmol/l) | 3.80±0.34 | 3.79±0.36 | .89 | 3.83±0.34 | 3.58±0.43 | .02 |
| Lactic acid, (mmol/l) | 1.26±1.20 | 1.37±1.03 | .62 | 1.29±0.81 | 0.94±0.22 | .11 |
| HDL-C, (mmol/l) | 29.23±3.90 | 28.46±3.77 | .31 | 29.02±3.80 | 26.26±3.14 | .01 |
| eGFR, (ml/(min*1.73m$^2$)) | 117.13±25.09 | 106.31±29.54 | .03 | 118.49±22.74 | 108.55±29.74 | .14 |
| Creatinine, (umol/l) | 65.30±19.22 | 69.14±33.25 | .35 | 64.35±14.09 | 70.31±21.95 | .17 |
| LDL-C, (mmol/l) | 24.46±1.84 | 24.51±2.49 | .89 | 24.37±1.77 | 24.56±2.44 | .73 |
| ALT, (U/l) | 25.03±18.11 | 29.23±19.50 | .24 | 29.72±22.25 | 36.08±35.10 | .36 |
| AST, (U/l) | 24.61±19.05 | 37.50±25.24 | <.001 | 24.56±12.24 | 37.51±23.90 | <.001 |
| Dyspnea | 6 (2) | 2 (7) | .18 | 2 (2) | 5 (36) | <.001 |
| Diabetes | 14 (5) | 3 (10) | .31 | 4 (4) | 3 (21) | .01 |
| Antivirals | 161 (56) | 29 (97) | <.001 | 73 (66) | 13 (93) | .04 |
| Exudative lesions | 50 (17) | 10 (33) | .07 | 16 (14) | 2 (14) | .99 |
| CAD | 5 (2) | 4 (13) | <.001 | 0 (0) | 0 (0) | - |

Data are number (percentage) or mean±SD. ALT, alanine aminotransferase; APTT, activated partial thrombin time; AST, aspartate aminotransferase; CAD, coronary heart disease; eGFR, estimated glomerular filtration rate; HDL–C, high density liptein cholesterol; LDL–C, low density lipoprotein cholesterol; PCO2, partial pressure of carbon dioxide; PCT, procalcitonin; PO2, partial pressure of oxygen; NTPRO-BNP, NT pro B-type natriuretic peptide; PT, prothrombin time.

segmenting image details is not as high as that achieved after object detection using the 2D network. As a result, the 2D network was chosen over the 3D network. Hoori et al. [7] proposed an EAT segmentation method using the DeepLab-v$^3$-plus technique. This method adds the learning of multi-scale features to improve the segmentation performance. Commandeur et al. [8] combined pericardium detection to segment the EAT. However, these methods are segmented in CT slices containing the heart, and the CT slices that do not contain the heart still had to be manually removed. Our proposed method demonstrated superiority over existing methods in two cohorts, attributed to the influence of negative samples provided by the object detection module prior to segmentation, which improved segmentation accuracy.

**Supplementary Table 2.** Features used in diagnostic models. The F features were ranked according to the AUC in univariate analysis

| Features of the source | Features |
|---|---|
| EAT | original_glszm_ZoneEntropy |
| Lung | original_firstorder_Kurtosis |
| Lung | original_glszm_SmallAreaEmphasis |
| EAT | original_firstorder_Skewness |
| Lung | original_glszm_LargeAreaLowGrayLevelEmphasis |
| EAT | original_glszm_LargeAreaLowGrayLevelEmphasis |
| Lung | original_glcm_MaximalCorrelationCoefficient |
| EAT | original_glszm_ZonePercentage |
| Lung | original_ngtdm_Strength |
| Lung | original_ngtdm_Complexity |


ISSN 0022-9040. Кардиология. 2024;64(9). DOI: 10.18087/cardio.2024.9.n2685

**Supplementary Figure 1.** Feature importance scores

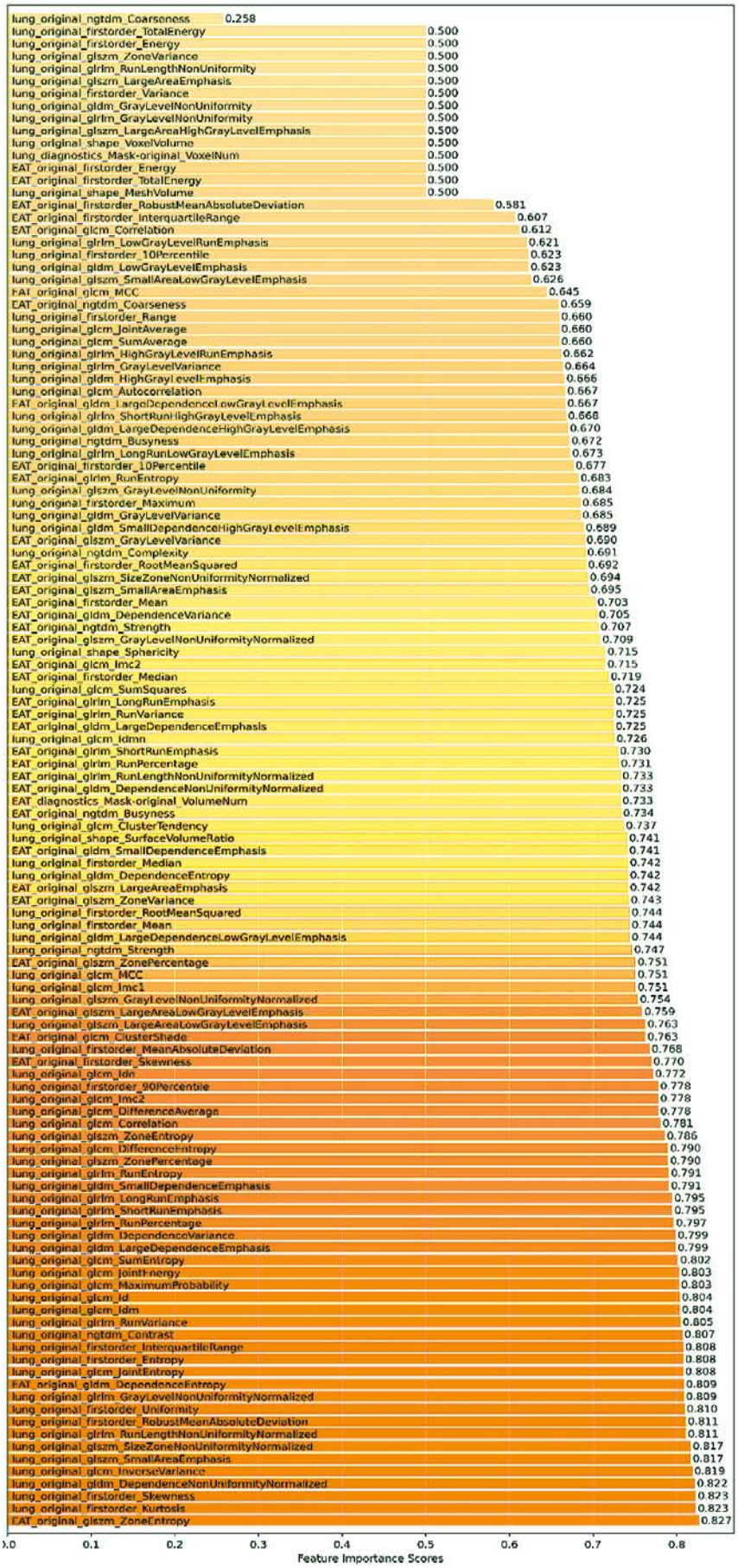


The left side of the bar shows the name of each feature,
and the right side of the bar shows the importance score of the corresponding feature.

Notably, the operational time for segmenting and extracting EAT from a patient's chest CT data on a standard computer was less than 20 seconds, a significant reduction compared to the approximately 20 minutes required for manual extraction by a specialist. This efficiency improvement represents a substantial time-saving advantage, facilitating more convenient EAT extraction and meaningful research endeavors.

### *Limitations*

Our study still has a few limitations. Firstly, in the segmentation model, two segmentation models need to be trained to complete the segmentation of the heart contour due to the imaging difference between the two centers' data. Secondly, the number of patients included in the study was relatively small.